Journal of Applied Mathematics and Physics (ZAMP)
Vol. 25, 1974 Birkhäuser Verlag Basel

On a Curve Veering Aberration

By Arthur W. Leissa[1]), Swiss Federal Institute of Technology, Zurich

1. Introduction

More than a decade ago, the writer came across a paper [1] which dealt with the free vibrations of rectangular cantilever plates. Classical plate theory, upon which the paper was based, and rectangular cantilever plates in particular, have been the subject of scores of other technical papers, both theoretical and experimental, and their behavior is widely understood and accepted. In addition to presenting voluminous numerical results for free vibration frequencies, the paper depicted a most astonishing behavior. Curves were plotted which showed the variation of frequency with the nondimensional aspect ratio of length to width for the plate. The curves behaved smoothly everywhere except where they approached each other. Then, instead of continuing smoothly and crossing, they each suddenly and violently veered away from the other (see, for example, Figure 1) and continued along the path that the other would have taken had it been permitted to cross!

The authors [1] call the regions 'transition zones' where the veering away occurs. Furthermore, because if the curves *did* cross, the same basic mode shape of free vibration would be associated with a curve before and after crossing, in the 'transition zones' of veering away the mode shapes and nodal patterns must undergo violent change—figuratively speaking, a dragonfly one instant, a butterfly the next, and something indescribable in between. Thus the results appear strange from an esthetic viewpoint.

One then wonders whether an error may not be present. But the plate theory is used correctly, even the free corner conditions which are so often overlooked. An exact solution to the problem is out of the question, but the paper uses a very powerful generalized Fourier method developed by A. E. Green [2], and uses it with obvious skill and understanding. Of course, the solution would require finding the roots of determinants of infinite size, but the authors have successively truncated to determinants of very large (although finite) order, have carried out all calculations on the computer in high precision, and claim that the results have converged. Because the results look magnificent everywhere except at the 'transition zones', it is difficult to dispute this claim.

Subsequently, a monograph [3] was prepared which summarized the literature of

[1]) On leave from Ohio State University, Columbus, Ohio, USA.

the world in plate vibrations. During the course of this work, a number of other references were found which exhibited the 'curve veering' aberration. In [4, 5] Claassen and Thorne applied the methods of [1] to two rectangular plates having other boundary conditions: (1) completely clamped and (2) clamped on two opposite edges, free on the two others. In [6, 7] the skew cantilever plate was analyzed. Earlier, Warburton [8] used a two-term Ritz solution with beam functions to analyze rectangular plates having various edge conditions. Huffington [9] did likewise for an orthotropic, rectangular plate. Mindlin et al. [10, 11, 12, 13] used a sixth order plate theory incorporating shear deformation effects to analyze thick circular and rectangular plates. In this latter work the 'curve veering' phenomenon was found to occur even though the solutions were *exact*.

For a rectangular plate there are 21 distinct cases [3] having clamped, simply supported, or free boundaries. It is widely known (cf., [3, 14, 15, 16]) that exact solutions to the classical theory exist for six of the cases—those having two opposite sides simply supported, while the other two edges can be any combination of clamped, simply supported, or free. It is generally understood, and during the research for [17] it was specifically verified, that the frequency curves (versus aspect ratio) always cross for these six cases. This raises the fundamental question: *Why do the six exact solutions yield crossings while the 15 approximate ones do not?* For, after all, from a physical vantage point, the six cases having exact solutions have all manner of edge conditions, as do the other 15 cases. Of course, the exact solutions permit a recognizable separation of the two independent space variables x and y, whereas no simple separation having a finite number of terms has been found for the other 15 cases; therefore, coupling exists in any of the latter known solutions when less than an infinite number of terms are retained in the solution.

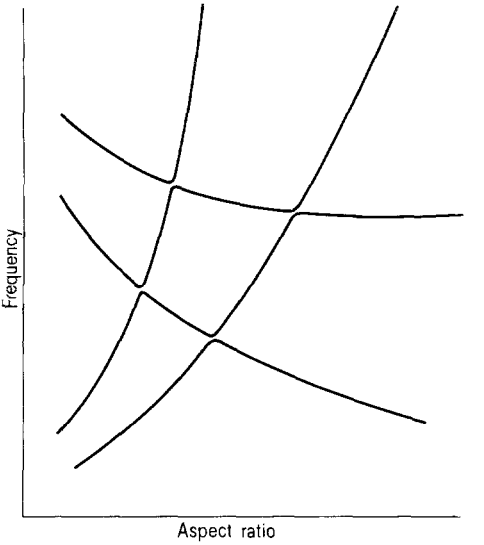

Figure 1
The 'curve veering' aberration.

Although the references described above all relate to the eigenvalue problem of free vibrations of plates, in recent years the writer has become keenly aware of the presence of the 'curve veering' phenomenon in other areas of mathematical physics where eigenvalue problems exist. Examples of such areas include:

1. Free vibrations of beams and shells.
2. Buckling of beams, plates, and shells.
3. Electromagnetic waves in waveguides.
4. Fluid flow in nonrigid conductors.
5. Potential curves and surfaces for molecules.

Because of the widespread apparent acceptance of the aberration the writer feels that it is time to examine the phenomenon more closely. He will begin to do so by looking at what is probably the most simple and best understood two-dimensional eigenvalue problem of mathematical physics—the free vibration of a rectangular membrane.

2. A Simple Example. Vibration of a Rectangular Membrane

Consider a rectangular flat membrane having dimensions $2a$ by $2b$, subjected to a uniform tension T. Making the usual assumptions of small transverse displacements, w, and constant mass density, ρ, the classical two-dimensional wave equation results,

$$T\nabla^2 w = \rho \frac{\partial^2 w}{\partial t^2} \tag{2.1}$$

where ∇^2 is the scalar Laplacian operator and t is time. Assuming free vibrations and a rectangular coordinate system x, y the displacement is expressed as

$$w(x, y, t) = W(x, y)e^{i\omega t} \tag{2.2}$$

where ω is the circular frequency. Introducing the nondimensional coordinates $\xi = x/a$ and $\eta = y/b$ and substituting (2.2) into (2.1) yields

$$\mathscr{L}(W) = \frac{\partial^2 W}{\partial \xi^2} + \left(\frac{a}{b}\right)^2 \frac{\partial^2 W}{\partial \eta^2} + \lambda^2 W = 0 \tag{2.3}$$

where λ^2 is a nondimensional parameter related to the frequency by

$$\lambda = \omega a \sqrt{\frac{\rho}{T}}. \tag{2.4}$$

Further, choosing the location of the ξ, η system so that the sides of the membrane are defined by $\xi = 0, 2$ and $\eta = 0, 2$, it is seen that the boundary conditions of zero displacement along all four sides are satisfied by choosing

$$W(\xi, \eta) = A_{mn} \sin \frac{m\pi\xi}{2} \sin \frac{n\pi\eta}{2} \tag{2.5}$$

where A_{mn} is an amplitude coefficient depending upon the initial conditions of the problem and m and n are integers. Substituting (2.5) into (2.3) yields

$$\lambda^2 = \left(\frac{\pi}{2}\right)^2\left[m^2 + \left(\frac{a}{b}\right)^2 n^2\right] \tag{2.6}$$

and the eigenvalue problem is solved exactly. The eigenvalues λ are given explicitly by (2.6) and the eigenfunctions by (2.5). It is seen further that if λ^2 is plotted versus the square of the aspect ratio, (2.6) determines a family of curves, depending upon the choice of m and n, all of which are straight lines. Three of these, corresponding to $mn = 11$, 13, and 31 are depicted by the dashed straight lines of Figure 2. The odd integers of m and n are chosen in order to yield only those free vibration mode shapes which are doubly symmetric with respect to the symmetry axes ($\xi = 1, \eta = 1$) of the rectangle, for it is generally accepted among proponents of the 'curve veering' aberration that, where symmetry exists, it can only occur between curves belonging to the same symmetry class of eigenfunctions. In Figure 2, as well as from (2.6), it is seen that the eigenvalues λ_{11}^2 and λ_{31}^2 lie on parallel straight lines, whereas the lines for λ_{31}^2 and λ_{31}^2 cross at $a/b = 1$, yielding a repeated eigenvalue for the square membrane.

3. An Approximate Solution. The Same Problem

Let us now see what happens when the problem of the previous section is solved by an approximate method. The well-known Galerkin method will be used in a quite

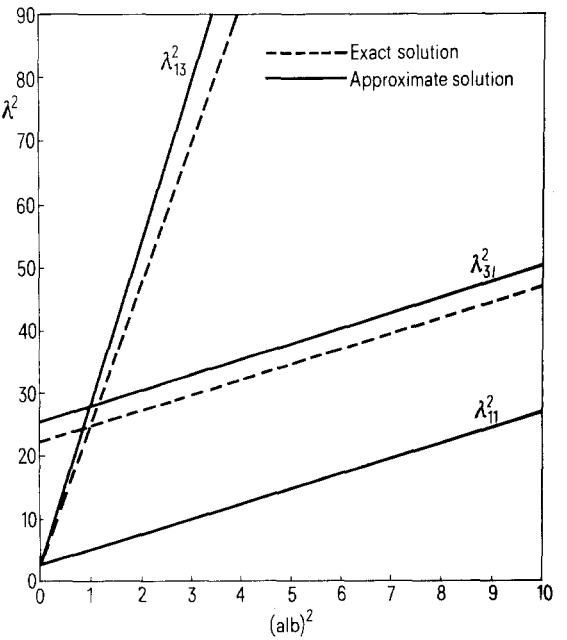

Figure 2
Eigenvalues versus aspect ratio.

straightforward and obvious way. For this problem the method is mathematically identical to the equally well-known Ritz method [18, 19].

If the origin of the ξ, η coordinate system is now chosen to be at the center of the rectangular region, it is clear that the boundary conditions $W = 0$ are satisfied exactly on all four sides by taking the algebraic polynomial

$$W = (\xi^2 - 1)(\eta^2 - 1) \sum_{i,j}^{M,N} a_{ij} \xi^i \eta^j \tag{3.1}$$

where i and j are integers $0, 1, 2, \ldots$ having upper limits M and N, respectively, and the a_{ij} are undetermined coefficients.

The Galerkin method consists of requiring the residual of the governing differential equation (2.3) to be made orthogonal to each term of the trial function (3.1) over the area

$$\int_A W_{pq} \mathscr{L}(W) dA = 0 \tag{3.2}$$

where W_{pq} is the term of (3.1) obtained by letting $i = p$ and $j = q$. Substituting (2.3) and (3.1) into (3.2) yields

$$\begin{aligned} \sum_{i,j}^{M,N} a_{ij} \Bigg\{ & \frac{1}{(j+q+5)(j+q+3)(j+q+1)} \\ & \times \left[\frac{(i+2)(i+1)}{i+p+3} - \frac{2(i^2+i+1)}{i+p+1} + \frac{i(i-1)}{i+p-1} \right] \\ & + \left(\frac{a}{b} \right)^2 \frac{1}{(i+p+5)(l+p+3)(i+p+1)} \\ & \times \left[\frac{(j+2)(j+1)}{j+q+3} - \frac{2(j^2+j+1)}{j+q+1} + \frac{j(j-1)}{j+q-1} \right] \\ & + \lambda^2 \frac{8}{[(i+p+5)(i+p+3)(i+p+1)][(j+q+5)(j+q+3)(j+q+1)]} \Bigg\} \\ = 0. & \end{aligned} \tag{3.3}$$

Thus, $(M + 1) \times (N + 1)$ simultaneous, homogeneous, linear algebraic equations in the unknown coefficients a_{ij} are generated by (3.3). For a non-trivial solution the determinant of the coefficient matrix is set equal to zero. For each fixed aspect ratio, a/b, the determinant yields $(M + 1) \times (N + 1)$ roots for the eigenvalues, λ^2.

For the rectangular membrane there are four symmetry classes of mode shapes, considering modes which are symmetrical or antisymmetrical with respect to the ξ and η axes. In this example, only the doubly symmetric modes will be used, as in the previous section. This is accomplished by retaining only the terms in (3.1) which are *even* in ξ and η (i.e., $i, j = 0, 2, 4, \ldots$). Considering the first three doubly symmetric terms within the summation sign of (3.1) $(i, j = 0, 2)$ then (3.3) yields a third order determinant for $p, q = 0, 2$:

$$|f_{ij}| = 0 \tag{3.4}$$

where

$$
\begin{aligned}
f_{11} &= 14\lambda^2 - 35(a/b)^2 - 35 \\
f_{22} &= \tfrac{2}{3}\lambda^2 - \tfrac{5}{3}(a/b)^2 - 11 \\
f_{33} &= \tfrac{2}{3}\lambda^2 - 11(a/b)^2 - \tfrac{5}{3} \\
f_{12} &= f_{21} = 2\lambda^2 - 5(a/b)^2 - 7 \\
f_{13} &= f_{31} = 2\lambda^2 - 7(a/b)^2 - 5 \\
f_{23} &= f_{32} = \tfrac{2}{7}\lambda^2 - (a/b)^2 - 1.
\end{aligned} \tag{3.5}
$$

The eigenvalues λ^2 of (3.4) are determined with a digital computer using an iterative root-finding program. However, when only the first term ($i = j = 0$) of (3.1) is retained, the resulting characteristic equation is obtained by truncating (3.4) to retain only f_{11}. Then $f_{11} = 0$, which yields

$$\lambda^2 = 2.5\left[1 + \left(\frac{a}{b}\right)^2 n^2\right]. \tag{3.6}$$

Comparing (3.6) with the exact eigenvalues (2.6) shows that the one-term representation, using parabolas to replace sine waves, is in itself reasonably accurate, yielding an upper bound for the lowest eigenvalue λ^2 which is everywhere within 1.3 per cent of the exact value, and a frequency ω which is everywhere within 0.7 per cent of the exact value. From this very good one-term solution, one can expect even better results when three terms are retained.

The results for the three-term solution are depicted by the solid lines in Figure 2. The curve for the lowest eigenvalue appears also to be a straight line which falls, for plotting purposes, on top of the curve for the exact solution. These eigenvalues are compared in Table 1. The results are given to six significant figures, although they were calculated to even greater accuracy, as will be demonstrated later.

Table 1
Comparison of the exact (2.6) lowest eigenvalues with those of the three-term solution

Solution type	$(a/b)^2$				
	0.1	0.5	1	2	10
Exact	2.71414	3.70110	4.93480	7.40220	27.1414
Three-term	2.71423	3.70122	4.93497	7.40245	27.1423

The curves for the higher two approximate eigenvalues λ_{31}^2 and λ_{13}^2 appear in Figure 2 also to be straight, parallel to and rotated from, respectively, the corresponding exact straight lines. These eigenvalues are seen to be significantly greater than the exact values in general, as might be expected for the higher modes of a Ritz-Galerkin solution. The lines appear to cross also at $(a/b)^2 = 1$. Indeed, if these curves were plotted with as many as 1000 equally-spaced data points (but carefully omitting the points for $a/b = 1.00$) for each curve, no other conclusion could be reached.

Suppose then one looks even more carefully in the interval $0.95 \leq (a/b)^2 \leq 1.05$. Enlarging Figure 2 a hundred times in this interval yields the view seen in Figure 3, where only the eigenvalue curves for the three-term approximate solutions for λ_{31}^2 and λ_{13}^2 appear. Here it is observed that the lines remain essentially straight *outside of* the interval $0.99 < (a/b)^2 < 1.01$, but that inside this interval, *they veer away from each other.*

The behavior of the curves in the 'transition zone' is further clarified by Table 2 wherein the eigenvalues in the interval $0.995 \leq (a/b)^2 \leq 1.005$ are displayed. From

Table 2
Eigenvalues and their second differences in the 'transition zone'

$\left(\frac{a}{b}\right)^2$	Upper curve		Lower curve	
	λ^2	Second difference	λ^2	Second difference
0.995	28.0285	—	27.8963	—
0.996	28.0328	0.0008	27.9201	−0.0008
0.997	28.0379	0.0013	27.9431	−0.0014
0.998	28.0443	0.0023	27.9647	−0.0023
0.999	28.0530	0.0033	27.9840	−0.0033
1.000	28.0650	0.0040	28.0000	−0.0040
1.001	28.0810	0.0034	28.0120	−0.0033
1.002	28.1004	0.0022	28.0207	−0.0023
1.003	28.1220	0.0014	28.0271	−0.0013
1.004	28.1450	0.0007	28.0322	−0.0009
1.005	28.1687	—	28.0364	—

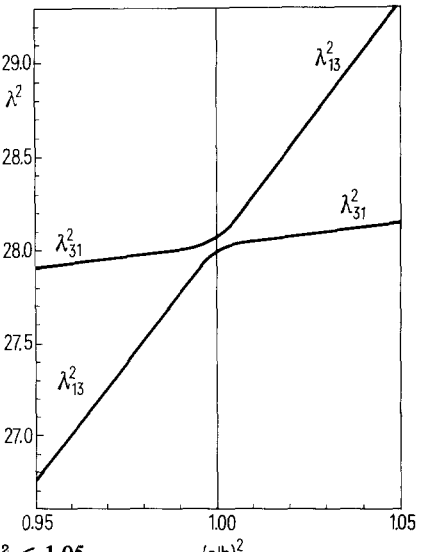

Figure 3
Enlarged view of Figure 2 for the interval $0.95 \leq (a/b)^2 \leq 1.05$.

these data it is seen that the curves appear to approach each other most closely at $(a/b)^2 = 1$ before veering away, and that the difference between the upper and lower curves at this point is approximately 0.2 per cent, too small to be identified in Figure 2. In Table 2 the second differences of λ^2, which are measures of the curvatures at the corresponding values of $(a/b)^2$, are also given. The positive and negative curvatures of the two curves are seen to increase significantly in magnitude as the points corresponding to $(a/b)^2 = 1.000$ are approached from either direction.

Thus the strange aberration of 'veering away' has been generated in a straightforward way on an otherwise well-behaved and well-understood problem. One may find it difficult to believe that the simple algebraic polynomial of (3.1), especially with only its first three terms, is capable of creating such a disturbance at $(a/b)^2 = 1$. Indeed, one may wonder whether apparent separation between the curves of Figure 3 is not due to numerical error in the computations.

Investigating the latter point, it is found that for $(a/b)^2 = 1$, the characteristic equation arising from the expansion of the determinant (3.4) using (3.5), can be written *exactly* in the partially factored form

$$(\lambda^2 - 28)(2\lambda^4 - 66\lambda^2 + 277) = 0 \tag{3.7}$$

yielding the roots $\lambda^2 = 28$ and $\frac{1}{2}(33 \pm \sqrt{535})$. The latter two roots were obtained to ten significant figure agreement with the iterative root-finding program used for the results of Table 2. Thus it is proven that the eigenvalue curves arising from the approximate solution do not cross but are represented accurately by Figure 3 and Table 2.

4. Mode Shapes and Their Contortions

An even more ugly behavior seen in the references of the Introduction, when the curve veering phenomenon is present, is the need for the eigenfunction mode shapes to alter themselves drastically in the so-called 'transition zones'. In terms of Figure 3 this means for the lower curve, for example, as the (a/b) ratio is increased, that the mode shape is the 13 mode for $(a/b)^2 < 0.99$ and the 31 mode for $(a/b)^2 > 1.01$, and must somehow change itself rapidly and in a continuous manner in the narrow interval $0.99 \leq (a/b)^2 \leq 1.01$. This is no small feat when one remembers the completely different forms of the node line patterns (lines of $W = 0$) associated with the two modes. These forms are depicted in Figure 4.

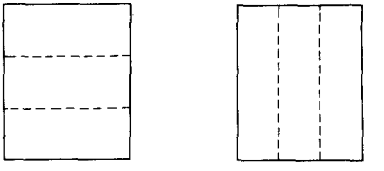

(a) 13 mode (b) 31 mode

Figure 4
Nodal patterns for the 13 and 31 modes.

To determine the nodal patterns corresponding to the three-term solutions in the interval $0.99 \leq (a/b)^2 \leq 1.01$, any two of the three homogeneous equations yielding (3.4) are taken. Let us take the first two, and rewrite them as

$$\begin{aligned} f_{11} + f_{12}b_{20} + f_{13}b_{02} &= 0 \\ f_{12} + f_{22}b_{20} + f_{23}b_{02} &= 0 \end{aligned} \tag{4.1}$$

where $b_{ij} = a_{ij}/a_{00}$ and the f_{ij} are as previously defined in (3.5). Solving (4.1) for the amplitude ratios b_{ij},

$$\begin{aligned} b_{20} &= \frac{f_{11}f_{23} - f_{12}f_{13}}{f_{13}f_{22} - f_{12}f_{23}} \\ b_{02} &= \frac{f_{12}^2 - f_{11}f_{22}}{f_{13}f_{22} - f_{12}f_{23}}, \end{aligned} \tag{4.2}$$

the transverse deflection of the membrane is conveniently written in nondimensional form as

$$\frac{W}{a_{00}} = (\xi^2 - 1)(\eta^2 - 1)(1 + b_{20}\xi^2 + b_{02}\eta^2) \tag{4.3}$$

which completely determines the mode shape corresponding to a given value of the eigenvalue λ. A nodal pattern is obtained by determining the values of ξ and η for which W/a_{00} is zero.

The change in the nodal patterns in the interval $0.95 \leq (a/b)^2 \leq 1.00$ for the lower curve of Figure 3 is depicted in Figure 5. Therein, in order to emphasize the changes, only the first quadrant of the membrane is shown. The continuation of the

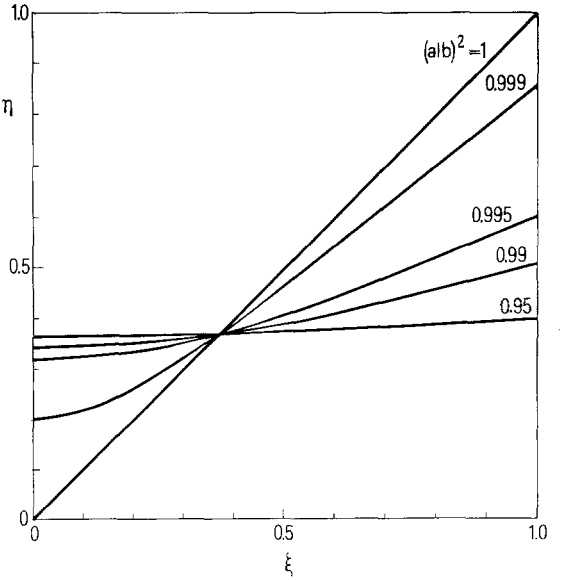

Figure 5
Nodal patterns corresponding to λ_{13}^2 for the interval $0.95 \leq (a/b)^2 \leq 1$.

nodal patterns into the other three quadrants is easily imagined by mentally reflecting the curves of Figure 5 about the ξ and η axes. It is seen that for $(a/b)^2 = 0.95$, the nodal pattern consists of two horizontal lines which are nearly straight, located at approximately $\eta = \pm 0.38$, which clearly identifies the pattern with the 13 mode. For the exact solution, the lines are straight and located at $\eta = \pm 0.33$, as in Figure 4a. However, it is seen that as $(a/b)^3 \to 1$, the curvature of the nodal lines at $\xi = 0$ continuously increases until, for $(a/b)^2 = 1$, the lines are found to be the diagonals of the square. The most rapid change in the nodal pattern occurs for $(a/b)^2 \geq 0.99$, where significant veering of the frequency curves begins. The effect appears even more drastic when one remembers that $(a/b)^2 = 0.99$ corresponds to $a/b = 0.995$.

The similar drastic change in the 31 mode for $(a/b)^2 \geq 0.95$ is shown in Figure 6, wherein the nodal patterns arising from the approximate solution using three terms are indicated by solid lines. In this case for $(a/b)^2 = 0.95$ the nodal lines are clearly the 31 mode shown in Figure 4b, and change drastically with increasing $(a/b)^2$, becoming a circle for $(a/b)^2 = 1$.

Looking further at (4.3), the shape of the nodal curves in Figures 5 and 6 becomes clear. Equation (4.3) shows that the boundaries $\xi = \pm 1$ and $\eta = \pm 1$, as well as the curve

$$b_{20}\xi^2 + b_{02}\eta^2 + 1 = 0 \tag{4.4}$$

are lines of zero deflection. From (4.4) it is seen that when b_{20}, as calculated from (4.2), is positive and b_{02} is negative, (4.4) represents a family of hyperbolas, which are the curves of Figure 5. For $b_{20} = -b_{02} = \infty$ the hyperbola degenerates into the straight diagonals. As $(a/b)^2$ increases beyond the value of unity, b_{20} becomes negative

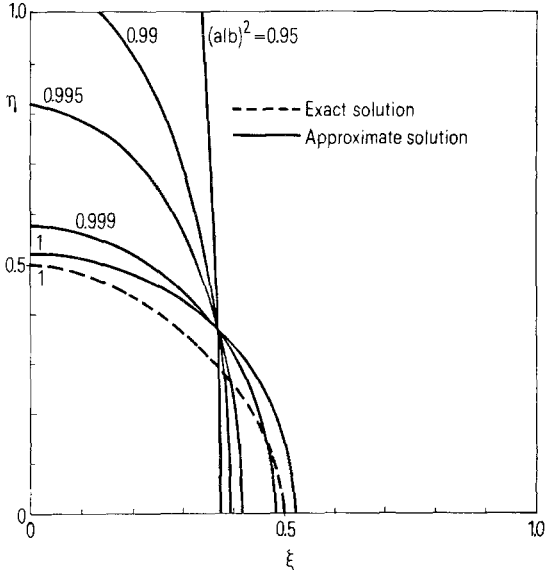

Figure 6
Nodal patterns corresponding to λ^2_{31} for the interval $0.95 \leq (a/b)^2 \leq 1$.

and b_{02} positive, generating a family of hyperbolas which are identical to those of Figure 5, but rotated about the diagonals, the separate curves then corresponding to $(b/a)^2 = 0.999$, 0.995, 0.99, and 0.95. Similarly, for b_{20} and b_{02} both negative in (4.4), and $b_{20}/b_{02} \geq 1$, (4.4) represents a family of ellipses, which are the curves of Figure 6. For $b_{20}/b_{02} = 1$ the ellipse becomes the special case of a circle. And as $(a/b)^2$ increases beyond the value of unity, $b_{20}/b_{02} < 1$ and a corresponding set of ellipses is generated for $(b/a)^2 = 0.999$, 0.995, 0.99, and 0.95 which are the same shapes as those of Figure 6, but having their major axes along the ξ axis instead. Thus, the nodal patterns associated with the lower eigenvalue curve of Figure 3 are all hyperbolas, and those of the upper curve are all ellipses. It is interesting to note that all nodal curves pass through the common point $\xi = \eta = 0.3697$.

That the simple polynomials of (3.1) generated by taking only the first three terms within the summation sign yield simple nodal patterns consisting of hyperbolas and ellipses should not be surprising. What is surprising is how rapidly these curves change their shape as they approach $(a/b)^2 = 1$ where the *exact* frequency curves cross. This is exactly the same behavior exhibited by the nodal pattern curves of [1, 5] where approximate solutions were used.

While discussing the subject of mode shapes and nodal patterns, let us return briefly to the exact solution presented previously in Section 2. Therein the mode shapes are given by (2.5). If two modes have the same frequency, then the initial conditions of the free vibration problem can always be chosen to permit any linear superposition of the two modes. In particular, for the 31 and 13 modes of the square membrane, superposition gives

$$W = A_{31} \sin \frac{3\pi\xi}{2} \sin \frac{\pi\eta}{2} + A_{13} \sin \frac{\pi\xi}{2} \sin \frac{3\pi\eta}{2}. \tag{4.5}$$

Choosing the initial conditions so that $A_{31} = -A_{13}$, and remembering that the coordinate origin for (4.5) is located in one corner of the region, then it is easily seen that for $\xi = \eta$ and $\xi = 2 - \eta$, the equations of the two diagonals, W is everywhere zero. Thus, one nodal pattern for the approximate solution for $a/b = 1$ can also be obtained from superposition of exact modes. Furthermore, taking $A_{31} = +A_{13}$ in (4.5), and employing some trigonometric identities, yields

$$\frac{W}{A_{31}} = 4 \sin \frac{\pi\xi}{2} \sin \frac{\pi\eta}{2} \left(\cos^2 \frac{\pi\xi}{2} + \cos^2 \frac{\pi\eta}{2} - \frac{1}{2} \right) \tag{4.6}$$

which is a product obtained from the equations of the edges of the membrane and an internal nodal line which is almost circular. This near-circle falls inside the nodal circle of the approximate solution, as shown in Figure 6.

Thus it has been shown that mode shapes of exact solutions can be superimposed to obtain mode shapes similar to those of an approximate solution. But the converse is not true. The approximate mode shapes cannot be superimposed in order to obtain

the natural mode shapes of an exact solution because, in order to do so, the mode shapes must have the same frequency; i.e., the frequency curves must cross.

5. Some Further Observations

In the preceding two sections of this work, the 'curve veering' aberration is seen to occur in an approximate solution. Its presence here is particularly disturbing because it is made to occur in a problem which has a very well-behaved exact solution. Furthermore, the aberration is seen to occur with greater severity than in any of the numerous references described in the Introduction.

It is clear in the present case that the aberration of reality occurs because of the application of an approximate method. Yet the method is the one most widely used on plate vibration problems [3] and is applied to the present problem in a most straightforward manner.

It can be seen from the present example that the aberration may imply *coupling when there is none.* In the example problem, the approximate solution eigenfunction (4.3) is, of course, representable by an infinite Fourier series, typical terms of which are the *exact* eigenfunctions (2.5), thus introducing hypothetical coupling among the exact eigenfunctions.

The writer will show in subsequent publications elsewhere that the 'curve veering' aberration occurs in many places in the solution of eigenvalue problems of mathematical physics. He also intends to demonstrate that the aberration is, in general, the result of approximation, and that the approximation can be induced in many ways. The effects of one approximate *method* are shown above. Approximations can also be caused by errors in numerical calculations.

Perhaps most importantly, the approximation causing the aberration may occur in the mathematical model (i.e., differential equation and boundary conditions) of a physical phenomenon. That is, the aberration can arise from the *exact* solution of a problem defined by an inadequate mathematical model. The latter should come as no great surprise, for the improvement of a mathematical model naturally comes from the observation of its deficiencies over some range of one's spectrum of interest.

References

[1] R. W. Claassen and C. J. Thorne, *Vibrations of a Rectangular Cantilever Plate*, J. Aerospace Sci. *29*, 1300–1305 (1962).
[2] A. E. Green, *Double Fourier Series and Boundary Value Problems*, Proc. Cambridge Phil. Soc., 1944.
[3] A. W. Leissa, *Vibration of Plates*, NASA SP-160, U.S. Government Printing Office, 1969.
[4] R. W. Claassen and C. J. Thorne, *Vibrations of Thin Rectangular Isotropic Plates*, J. Appl. Mech. *28*, 304–305 (1961).
[5] R. W. Claassen and C. J. Thorne, *Transverse Vibrations of Thin Rectangular Isotropic Plates*, NOTS Tech. Pub. 2379, NAVWEPS Rept. 7016 U.S. Naval Ordnance Test Sta., China Lake, Calif., Aug. 1960. (Errata available from CFSTI as AD 245 000.)
[6] R. W. Claassen, *Vibration of Skew Cantilever Plate*, Pacific Missile Range Tech. Rept. PMR-TR-62-1, Pacific Missile Range, May 1963.

[7] R. W. CLAASSEN, *Vibrations of Skew Cantilever Plates*, AIAA J. *1*, 1222 (1963).
[8] G. B. WARBURTON, *The Vibration of Rectangular Plates*, Proc. Inst. of Mech. Engrs. *168*, 371 (1954).
[9] N. J. HUFFINGTON, Jr., *On the Occurrence of Nodal Patterns of Nonparallel Form in Rectangular Orthotropic Plates*, J. Appl. Mech., Brief Notes, *28*, 459–460 (1961).
[10] R. D. MINDLIN and H. DERESIEWICZ, *Thickness-Shear and Flexural Vibrations of a Circular Disk*, J. Appl. Phys. *25*, 1329–1332 (1954).
[11] H. DERESIEWICZ and R. D. MINDLIN, *Axially Symmetric Flexural Vibrations of a Circular Disk*, J. Appl. Mech. *22*, 86–88 (1955).
[12] H. DERESIEWICZ, *Symmetric Flexural Vibrations of a Clamped Circular Disk*, J. Appl. Mech. *23*, 319 (1956).
[13] R. D. MINDLIN, A. SCHACKNOW and H. DERESIEWICZ, *Flexural Vibrations of Rectangular Plates*, J. Appl. Mech. *23*, 430–436 (1956).
[14] W. VOIGT, *Bemerkungen zu dem Problem der transversalen Schwingungen rechteckiger Platten*, Nachr. Ges. Wiss. (Göttingen) *6*, 225–230 (1893).
[15] S. IGUCHI, *Die Eigenwertprobleme für die elastische rechteckige Platte*, Mem. Fac. Eng., Hokkaido Univ., 305–372 (1938).
[16] H. J. FLETCHER, *The Frequency of Vibration of Rectangular Isotropic Plates*, J. Appl. Mech. *26*, 290 (1959).
[17] A. W. LEISSA, *On Vibration of Rectangular Plates*, Journal of Sound and Vibration (to be published).
[18] L. V. KANTOROVICH and V. I. KRYLOV, *Approximate Methods of Higher Analysis* (English. translation: P. Noordhoff, Groningen 1964).
[19] A. W. LEISSA, W. E. CLAUSEN, L. E. HULBERT and A. T. HOPPER, *A Compansion of Approximate Methods for the Solution of Plate Bending Problems*, AIAA J. *7*, 920 (1969).

Abstract

In numerous places in the literature of eigenvalue problems of mathematical physics one finds curves which approach each other and suddenly veer away. The author postulates that this ugly behavior may be the result of approximation in the representation of physical reality. In the present paper such behavior is demonstrated to arise from the application of the well-known Ritz-Galerkin method to the classical eigenvalue problem of the free vibration of a rectangular membrane.

Zusammenfassung

An vielen Stellen der Literatur über Eigenwertprobleme der mathematischen Physik kommen Kurven vor, die sich nähern, aber bevor sie sich schneiden, wieder auseinander laufen. Der Verfasser postuliert, dass dieses unschöne Verhalten durch die Approximation in der Erfassung der physikalischen Wirklichkeit verursacht werden kann. In der vorliegenden Arbeit wird als Beispiel die klassische Eigenwertaufgabe der schwingenden Rechteckmembrane gewählt und durch Anwendung des Verfahrens von Ritz-Galerkin ein derartiges Verhalten nachgewiesen.

(Received: June 6, 1973)